Proceedings of the 2010 3rd IEEE RAS & EMBS
International Conference on Biomedical Robotics and Biomechatronics,
The University of Tokyo, Tokyo, Japan, September 26-29, 2010

A Meshless Framework For Bevel-tip Flexible Needle Insertion Through Soft Tissue

Jijie Xu[1], *Member*, Linwei Wang[2], Ken C.L. Wong[2], and Pengcheng Shi[2], *member*

***Abstract*— Flexible needle offers greater mobility and maneuverability in minimally invasive procedures. However, its nonholonomic property and complicated interactions with soft tissues makes accurate insertion and motion planning for this type of needle still a challenge. Realistically modeling and simulating its insertion through a soft tissue will provide many information to enhance the motion planning and control of the flexible needle.This paper presents a meshless framework for modeling and simulation of flexible needle insertion through soft tissue. Instead of using elements to represent the needle and soft tissue as in most existing FEM-based methods, which are connected with meshes, our approach uses two separated sets of nodes to represent them. Structure constraints as used in FEM-based methods have been released, and the needle interacts with the soft tissue using a moving least square approximation. Since no mesh is required in this approach, no remeshing or mesh modification is needed for both accuracy refinement and tissue-needle interaction. Finally, simulations results are provided to validate the performance of our approach.**

I. Introduction

Motion planning for the flexible needle is important in order to perform accurate insertion. Several approaches have been developed to apply the state-of-the-art motion planning algorithms on the flexible needle [1], [2], [3]. However, most of them are based on the assumption of rigid workspace, which greatly restricts their usability in clinical applications. Although attempts have been made to solve the motion planning problem in a deformable environment, only deformable robot and obstacles were modeled and considered in the planning procedure [4]. A framework that realistically models and simulates deformation of the soft tissue as well as the movements of the needle will be a foundation to ultimately solve the motion planning of flexible needle in real applications.

Most existing modeling and simulations for needle insertions are developed based on FEM, for which the spatial domain of both the tissue and the needle is discretized into a mesh of finite elements [5]. FEM-based approaches usually require remeshing or mesh modification for the needle insertion. Remeshing procedure is usually theoretically complicated and computational expensive, especially for high-order elements which possess higher numerical accuracy than linear elements. Mesh modification, on the other hand, use local adjustment of existing nodes to approximate the needle's motion, which reduce the computational cost but sacrifice accuracy.

This paper presents some preliminary results of our work, whose ultimate goal is to solve motion planning for the flexible needle insertion in soft tissue. We develop a framework to model and simulate insertion of the flexible needle in soft tissue based on meshless approaches [6]. Instead of representing the soft tissue and the needle as connected elements by mesh, we use a set of unstructured nodes bounded by the tissue boundary to model the soft tissue, and use another set of nodes to model the flexible needle exactly following its kinematic characteristics. Deformation and stress on the tissue is calculated using the moving least square approximation (MLSA). As no mesh is needed, node distribution can be easily refined for numerical accuracy, and no remeshing is required for the needle insertion. Moreover, since the needle will exactly follow its kinematics, this framework can be further applied to solve the motion planning of the flexible needle.

II. Related Work

Webster et al. [7] showed experimentally that steerable bevel-tip needles follow paths of constant curvature in the direction of the bevel-tip, and the radius of that curvature is not significantly affected by the insertion velocity. They also developed a nonholonomic model of the needle's motion in stiff tissues based on a generalized bicycle model and fit model parameters using experiments with tissue phantoms [8]. By modeling the bevel tip needle's motion in a 2D workspace as a non-reversible Dubins car, Alterovitz et al. [9] formulated the 2D steerable needle motion planning problem as a nonlinear optimization problem. They further formulated the motion planning problem as a Markov Decision Process (MDP) [10] and proposed the Stochastic Motion Roadmap (SMR) to search for the plan with most probability of success [11]. For clinical implementation, research on steerable needle insertion has been extended to more complex 3D environments in many different ways [12][13]. By representing the bevel-tip needle's 3D motion as a screw motion, Duindam et al. [1] formulated 3D motion planning problem for the steerable needle as a dynamical optimization problem with a discretized control space. Based on the inverse kinematics and the self-motion manifold of the steerable needle, they also presented a local motion planning algorithm for steerable needle in 3D environment by solving the Paden-Kahan subproblems [14]. Inspired by the Rapidly-exploring Random Tree (RRTs) algorithms, Xu

1. The author is with the Human Engineering Research Laboratories, University of Pittsburgh, Pittsburgh, PA, USA. E-mail: jix33@pitt.edu

2. The authors are with the PhD program in Computing and Information Sciences, B. Thomas Golisano College of Computing and Information Science, Rochester Institute of Technology, Rochester, NY, USA.

978-1-4244-7709-8/10/$26.00 ©2010 IEEE

et al. [2] developed the first specific 3D sampling-based motion planner for the steerable needle insertion, and further presented a method to plan a "fireworks" for multiple needles [3].

A breakthrough made by DiMaio et.al. presented a planar virtual environment for needle insertion, which was developed based on a static linear finite element model and estimated needle shaft forces and tissue behavior [15]. By non-rigidly aligning volumetric data sets to a physical mannequin surface, Magee et.al. developed a computer simulator to generate "virtual ultrasound" images using position of a mock ultrasound probe and needle [16]. Jiang et. al. presented a 3D model of needle insertion based on large deformation nonlinear dynamic FEM and Mooney-Rivlin material model [17]. Using quasi-static stick-slip friction for needle/tissue interactions, Nienhuys developed an FEM model for needle insertion in both 2D and 3D tissue and proposed iterative algorithms to handle nonlinear material properties of the tissue and adaptively refine the mesh near the needle trajectory [18]. Considering both geometric and material non-linearity, Wittek et. al. developed a approach to simulate needle insertion in brain tissue [19]. Remeshing was limited in a very small neighborhood around the needletip to insure good computational performance, which in some kind sacrifices some simulation accuracy.

However, specific characteristics of the flexible needle raise many new issues for needle insertion simulation. Considering the nonholonoic property of the flexible needle, Alterovitz et. al. modeled 2D soft tissue as a FEM mesh and simulate the needle as a 1D discretized curve composing of line segments. The trajectory of the needle is approximated by relocating a set of neighbored elements around the needle tip in the tissue mesh through mesh modification [20], [21]. Based on the tissue deformation simulated with this model, they further developed motion planning algorithms to senselessly plan the needle's trajectory in 2D environment using nonlinear optimization techniques. By coupling a 3D FEM simulation of tissue with a 1D inextensible needle, Chentanez et. al. recently introduced a novel interactive simulation for flexible needle insertion in 3D environment, which provided a quick local remeshing to enable accurate computation of contact forces but sacrifice some global accuracy [22].

FEM-based approaches usually suffer from high cost in mesh generation, low accuracy of stress, and difficulties in adaptive analysis and large deformations. To release from the restrictions of finite elements, meshfree methods have been applied in surgical modeling [23]. Another reason for us to choose meshless methods for needle insertion is that, after releasing the mesh, the needle can fully follow its kinematics or dynamics characteristics and need no mesh modification or remeshing, which makes it very compatible with the formation of the motion planning problem. To the best of our knowledge, this is the first meshfree framework developed for modeling and simulation of the flexible needle insertion.

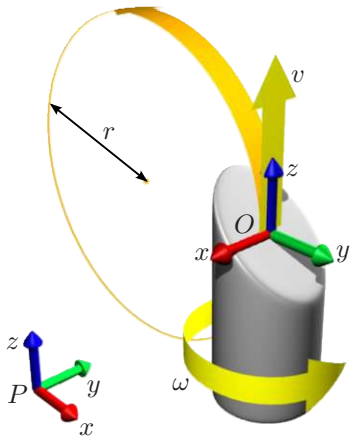

Fig. 1. Model of the bevel-tip needle.

III. Kinematics of Bevel-Tip Flexible Needle

Consider the bevel-tip needle shown in Fig. 1. Referring to the notations in [24], a spatial frame P is attached to the base of the needle and a body frame O is attached to the geometric center of the bevel tip. The configuration of the needle tip can be represented homogeneously by the 4-by-4 transformation matrix of the object frame relative to the spatial frame:

$$g_{PO} = \begin{bmatrix} R_{PO} & p_{PO} \\ 0 & 1 \end{bmatrix} \in SE(3),$$

where $R_{PO} \in SO(3)$ is the rotation matrix and $p_{PO} \in T(3)$ is the position of frame O relative to frame S.

The motion of the needle is fully determined by two motions of the bevel tip: insertion with velocity $v(t)$ in the z direction and rotation with velocity $\omega(t)$ about the z axis of the body frame O [8], [1]. It has been experimentally shown that the bevel-tip needle will follow a constantly curved path with curvature $\kappa = \frac{1}{r}$ while pushed with zero bevel rotation velocity, i.e. $\omega = 0$ [7] . The instantaneous velocity of the needle tip can be represented in the body frame O as

$$V_{PO}^b = [\mathbf{v}^T \quad \mathbf{w}^T]^T = [0 \quad 0 \quad v(t) \quad v(t)/r \quad 0 \quad \omega(t)]^T. \quad (1)$$

When V_{PO}^b is constant, i.e., $v(t)$ and $\omega(t)$ are constant, the configuration of the needle tip relative to the spatial frame after being pushed for a time interval t is

$$g_{PO}(t) = g_{PO}(0)e^{\hat{V}_{PO}^b t}, \quad (2)$$

where $g_{PO}(0)$ is the initial configuration of the needle frame relative to the spatial frame, and

$$\hat{V}_{PO}^b = \begin{bmatrix} 0 & -\omega(t) & 0 & 0 \\ \omega(t) & 0 & -v(t)/r & 0 \\ 0 & v(t)/r & 0 & v(t) \\ 0 & 0 & 0 & 0 \end{bmatrix}. \quad (3)$$

For constant V_{PO}^b, the needle motion can also be interpreted as a screw motion with constant axis and pitch [24], [1]. When the entire insertion of the needle is discretized into N time intervals $\{I_1, \cdots, I_N\}$ with $I_i = [t_{i-1}, t_i]$, with fixed

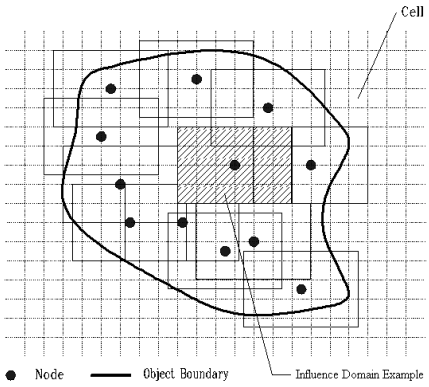

Fig. 2. Example of nodes and influence domains

velocity $V_{PO}^b(I_n)$ in each step, the final configuration of the needle tip can be computed as a product of exponentials:

$$g_{PO}(T) = g_{PO}(0)e^{\hat{V}_{PO}^b(I_1)I_1} \cdots e^{\hat{V}_{PO}^b(I_N)I_N}. \quad (4)$$

IV. Needle Insertion Modeling with Meshfree Method

For the meshfree method, instead of discretizing the spatial domain of the soft tissue into elements as in FEM, the tissue is represented by a set of unstructured nodes bounded by the tissue boundary. The n nodes, $\mathbf{x}_i = (x_i, y_i)$ for 2D and $\mathbf{x}_i = (x_i, y_i, z_i)$ for 3D, $i = 1, \ldots, n$, distributed over the tissue body Ω as shown in Fig. 2, contain the nodal values used to approximate the continuous field of the quantities of interest, such as displacements. The density of the nodes depends on the accuracy requirement and the available computational resources, and the nodal distribution can be either uniform or non-uniform with denser distributions in areas with large shape variation or large displacement gradient.

Since no mesh is required in the meshfree method, the relations between the nodes and any point within Ω are provided by the influence domains [6]. Every node is given an influence domain, and the values of any point in the tissue are approximated by the values of the nodes whose influence domains covering this point. Thus, the influence domains of all nodes together should cover the whole tissue.

A. Moving Least Square Approximation

There are different approaches to approximate the values of a point from the nodal values, among which the moving least square approximation has been adopted because of its relative ease of implementation, and its compatibility and consistency [6]. Compatibility means the approximated fields of values are smooth and continuous, and consistency means the approximated fields can exactly represent the polynomials of desired order.

Let u be a continuous scalar function defined over the tissue body Ω. For a point at $\mathbf{x} \in \Omega$, $u(\mathbf{x})$ can be given as:

$$u(\mathbf{x}) = \sum_{j=1}^{m} p_j(\mathbf{x}) a_j(\mathbf{x}) = \mathbf{p}^T(\mathbf{x})\mathbf{a}(\mathbf{x}), \quad (5)$$

where $p_j(\mathbf{x})$ are the monomial basis functions and $a_j(\mathbf{x})$ are coefficients to be determined. Without loss of generality, we use linear basis functions in this paper, i.e., for 2D tissue,

$$\mathbf{p}^T(\mathbf{x}) = \begin{bmatrix} 1 & x & y \end{bmatrix},$$

and for 3D tissue,

$$\mathbf{p}^T(\mathbf{x}) = \begin{bmatrix} 1 & x & y & z \end{bmatrix},$$

where (x, y, z) are the cartesian coordinates of $\mathbf{x}$ in 3D space. Let u_i be the value of node i located at $\mathbf{x}_i$, by minimizing the weighted, discrete L_2 norm:

$$L = \sum_{i=1}^{n} w(\mathbf{x} - \mathbf{x}_i) \left[\mathbf{p}^T(\mathbf{x}_i)\mathbf{a}(\mathbf{x}) - u_i\right]^2, \quad (6)$$

where $w(\mathbf{x} - \mathbf{x}_i)$ is the weight function, we have

$$\mathbf{a}(\mathbf{x}) = \mathbf{A}^{-1}(\mathbf{x}) \sum_{i=1}^{n} \mathbf{B}_i(\mathbf{x}) u_i \quad (7)$$

and thus:

$$u(\mathbf{x}) = \sum_{i=1}^{n} \left(\mathbf{p}^{\mathrm{T}}(\mathbf{x})\mathbf{A}^{-1}(\mathbf{x})\mathbf{B}_i(\mathbf{x})\right) u_i \equiv \sum_{i=1}^{n} \phi_i(\mathbf{x}) u_i \quad (8)$$

where

$$\mathbf{A}(\mathbf{x}) = \sum_{i=1}^{n} w_i(\mathbf{x})\mathbf{p}(\mathbf{x}_i)\mathbf{p}^{\mathrm{T}}(\mathbf{x}_i); \quad \mathbf{B}_i(\mathbf{x}) = w_i(\mathbf{x})\mathbf{p}(\mathbf{x}_i)$$

and ϕ_i is called the shape function of node i. $w_i(\mathbf{x}) \equiv w(\mathbf{x} - \mathbf{x}_i) \equiv w(r)$ is the cubic spline weight function, which is given as:

$$w(r) = \begin{cases} \frac{2}{3} - 4r^2 + 4r^3, & \text{for } r \le \frac{1}{2} \\ \frac{4}{3} - 4r + 4r^2 - \frac{4}{3}r^3, & \text{for } \frac{1}{2} < r \le 1 \\ 0, & \text{for } r > 1 \end{cases} \quad (9)$$

with $r = \|\mathbf{x} - \mathbf{x_i}\|/d_i$, the distance between $\mathbf{x}$ and $\mathbf{x_i}$ normalized by the size of the influence domain of node i (d_i). With (8), u and its derivatives can be approximated using the nodal values. This approximation can be used to solve the system equation for the tissue deformation, which does not have closed form solution in general.

B. Tissue Deformation

As the speed of the needle insertion is slow, the tissue deformation can be approximated by a static system. The relation between the external force and the deformation of the tissue can be described by the total potential energy, PE, which can be expressed as the difference between the strain energy of the tissue, E_s, and the work done by the external forces, W_f [5]:

$$PE = E_s - W_f. \quad (10)$$

Let $\mathbf{S}$ and $\boldsymbol{\epsilon}$ be the vectors containing the components of the stress and strain tensors respectively, as shown in Fig. 3, the strain energy over this solid body Ω is:

$$E_s = \frac{1}{2} \int_{\Omega} \boldsymbol{\epsilon}^T \mathbf{S} \, \mathrm{d}\Omega, \quad (11)$$

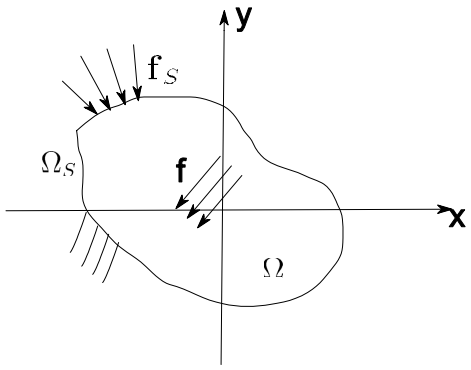

Fig. 3. A 2D soft tissue: Ω: tissue body; Ω_S: tissue boundary; $\mathbf{f}_S$: traction force; $\mathbf{f}$: external force.

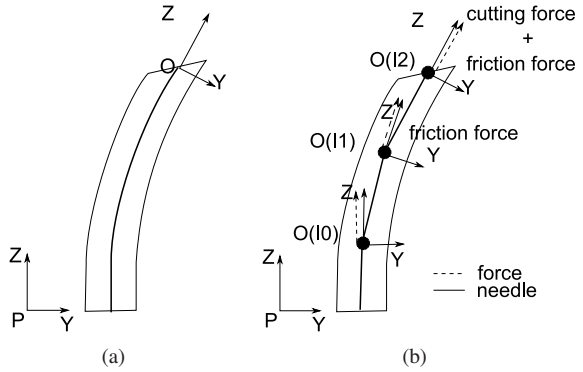

Fig. 4. Meshfree Model of Flexible Needle: (a). The needle is represented as an 1D curve in the workspace; (b). Meshfree model of the flexible needle: a set of nodes.

and the work done by external forces can be computed as:

$$W_f = \int_\Omega \mathbf{u}^T \mathbf{f} \, \mathrm{d}\Omega + \int_{\Omega_S} \mathbf{u}^T \mathbf{f}_S \, \mathrm{d}\Omega_S, \tag{12}$$

where $\mathbf{u}$ is the displacement, $\mathbf{f}$ is the body force, and Ω_S is the boundary of the tissue on which traction force $\mathbf{f}_S$ is applied.

Using MLSA, the displacement at a point can be approximated as $\mathbf{u}(\mathbf{x}) = \mathbf{\Phi}(\mathbf{x})\mathbf{U}$, where $\mathbf{\Phi}(\mathbf{x})$ is a matrix containing the shape functions $\phi_i(\mathbf{x})$, and $\mathbf{U}$ is a vector comprises nodal displacements of all nodes. Similarly, the strain-displacement relation is given as $\boldsymbol{\epsilon}(\mathbf{x}) = \mathbf{L}(\mathbf{x})\mathbf{U}$, where $\mathbf{L}(\mathbf{x})$ is a matrix containing the spatial derivatives of the shape functions, as the strain components are composed of the derivatives of the displacements [5]. Furthermore, the stress-strain relation is described by the Hooke's law $\mathbf{S}(\mathbf{x}) = \mathbf{D}\boldsymbol{\epsilon}(\mathbf{x})$, where $\mathbf{D}$ is a matrix of material constants, which are usually the *Young's modulus* (E) and *Poisson ratio* (ν) for linear material properties.

Since the minimum total potential energy principle requires $\delta PE = 0$, we have the matrix equation of Galerkin weak-form for the relation between displacements and external forces:

$$\left(\int_\Omega \mathbf{L}^T \mathbf{D} \mathbf{L} \, \mathrm{d}\Omega \right) \mathbf{U} = \int_\Omega \mathbf{\Phi}^T \mathbf{f} \, \mathrm{d}\Omega + \int_{\Omega_S} \mathbf{\Phi}^T \mathbf{f}_S \, \mathrm{d}\Omega_S. \tag{13}$$

In consequence, when the needle provides the external forces $\mathbf{f}$, the corresponding nodal displacements $\mathbf{U}$, and thus the deformation of the tissue, can be computed.

C. Needle Model

As discussed in Section III, the needle's motion is fully determined by the rotation control $\omega(I_i)$ and the insertion control $v(I_i)$ in each time interval I_i, as

$$V_{PO}^b(I_i) = [\mathbf{v}^T \quad \mathbf{w}^T]^T = [0 \quad 0 \quad v(I_i) \quad v(I_i)/r \quad 0 \quad \omega(I_i)]^T.$$

To simplify the modeling, we make the following reasonable assumptions: 1) the steerable needle is a rigid body sufficiently flexible, such that the needle is fully control by its control inputs; 2) the motion of the needle is fully determined by its tip, which means that the needle body follows the path of the needle tip. With these assumptions, how the needle moves in the plane is identical to motions of the body frame O. Therefore, we model the steerable needle as an 1 dimensional curve representing the trajectory of frame O in the workspace, as shown in Fig. 4-(a). With the discretized kinematics, the needle will travel from configuration $g_{PO}(t_i)$ to $g_{PO}(t_i)$ within a time interval I_i, and the dwelled configuration of O is selected as a node of the need. Collectively, the needle can be represented as a set of nodes as shown in Fig. 4-(b).

Using the needle insertion force model obtained in [25], the needle tip exerts both cutting force and friction force on the tissue, and other parts of the needle exert only friction force. By providing an influence domain for every needle node, the body force on a point $\mathbf{x}$ of the tissue can be computed as:

$$\mathbf{f}(\mathbf{x}) = \begin{cases} \left(1 - \frac{\|\mathbf{x} - \bar{\mathbf{x}}_i\|}{\bar{d}_i}\right) \bar{\mathbf{f}}_i, & \text{for } \|\mathbf{x} - \bar{\mathbf{x}}_i\| \le \bar{d}_i \\ \mathbf{0}, & \text{otherwise} \end{cases} \tag{14}$$

with $\bar{\mathbf{x}}_\mathbf{i}$, $\bar{d}_i$, and $\bar{\mathbf{f}}_i$ are respectively the position, influence domain, and body force of the needle node closest to this point. As the influence domains of the needle nodes are independent from those of the tissue nodes, no influence domain update is required during needle insertion. With $\mathbf{f}$ as the input to (13), the deformation of the tissue caused by the needle insertion can be computed.

V. Simulation Results

A. Flexible insertion in 2D soft tissue

We first simulate the flexible needle insertion in a 2D homogeneous and isotropic tissue. To develop the meshfree model of the tissue, we applied a uniform node distribution and a total of 961 nodes were sampled with average node space $d_{node} = \frac{L}{30}$, where $L = 180mm$ is the side length of the square. Each node has two degrees-of-freedom. Linear material property was considered and material constants experimentally derived in [15] were applied, with Young's modulus $E = 65$ kPa and Poisson ratio $\nu = 0.45$. The influence domain of every node was defined as a circle with radius $\alpha \cdot d_{node}$. In our simulation, we set $\alpha = 1.2$.

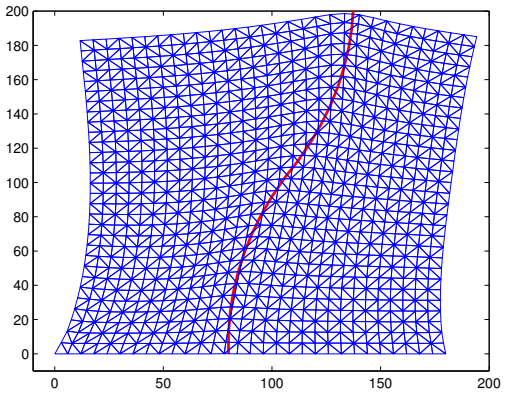

(a) step 18

Fig. 5. Flexible needle insertion in homogeneous 2D soft tissue. The needle is illustrated as connected line segments.

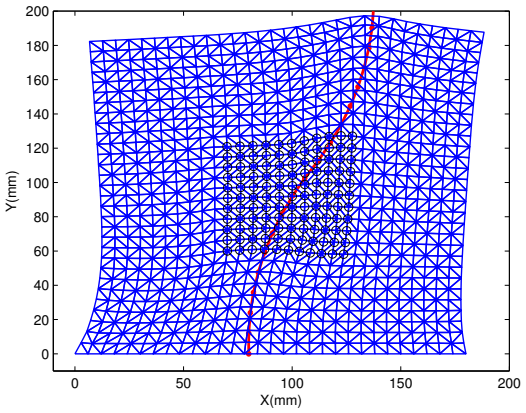

(a) step 18

Fig. 6. Flexible needle insertion in nonhomogeneous 2D soft tissue. The needle is illustrated as connected line segments.

However, different α can be used to describe more complicated connections between local nodes. The geometry of the 2D square tissue is shown in Fig. 5-(a). Notice that in real application, the skin for inserting the needle is usually pushed by a flat instrument to reduce tissue sliding during the procedure. Therefore, the bottom edge of the tissue is fixed in our simulation as the displacement boundary condition.

When the needle is inserted in 2D plane, the bevel-tip can only be rotated about its z-axis for 0^o or 180^o, which represent two bevel directions, bevel left or bevel right. The needle was inserted from an entry point located at (80mm, 0) with a constant insertion velocity $v(t) = 12$ mm/s with respect to the metric of the tissue for each time step of the simulation. The constant curvature of the needle's trajectory is $\kappa = \frac{1}{120}$. Initial bevel direction is **bevel right**, and the bevel-tip flips to **bevel left** at step 10 of the simulation. With the force model developed in [25], both cutting force and static friction force are applied at the bevel-tip node, and only a friction force is applied to each node on the needle body. Then displacements of tissue nodes were computed using (13) for each time step. Fig. 5 shows the bevel-tip flexible needle insertion in this homogenous 2D soft tissue. The bevel-tip is flipped in step 8.

We then simulate the flexible needle in a nonhomogeneous, isotropic 2D soft tissue, which has the same dimension as the homogeneous one. A 60mm by 60mm square part in the center has a Young's modulus $E = 650$ kPa, and the other part has the same properties as the homogeneous one. Same node distribution and influence domain is applied to build the meshfree model of this nonhomogeneous tissue, and the same needle model and force model is used. Fig. 6 shows the insertion with the same control as the previous one. Comparing with Fig. 5, we can see the effects of the nonhomogeneity during the inseriton. The simulation results obviously showed that the proposed meshfree approach can well handle homogeneity of the soft tissue.

B. Flexible needle insertion in 3D soft tissue

Last, we model and simulate the flexible needle insertion in a 3D cubic soft tissue, which is homogeneous and isotropic tissue. Similar to the 2D cases, we applied a uniform node distribution and 343 nodes were sampled with average node space $d_{node} = \frac{L}{30}$, where $L = 180$mm is the edge length of the cube. Same material properties as used in 2D cases are applied. The influence domain is a sphere with radius $1.2 \cdot d_{node}$. The geometry of the cubic tissue is shown in Fig. 7. The bottom face is fixed as the displacement boundary condition.

The needle was inserted from an entry point located at (60mm,60mm, 0) with a constant insertion velocity $v(t) = 12$ mm/s and the rotation velocity $\omega = 1\text{rad/s}$. The curvature that the needle's trajectory followed is $\kappa = \frac{1}{120}$, and initial bevel orientation is normal to the bottom face. An influence domain with the same dimension as the tissue nodes is defined for any node of the needle. In clinical needle insertion, the physician usually perform the insertion in a discretized strategy: first insert the needle with velocity v for a distance, and then rotate the needle with angular velocity ω for an angle. The insertion will be completed by repeat this procedure with different insertion depths and rotation angles. Therefore, we apply this control strategy to simulate the flexible needle insertion in 3D soft tissue. At step 5, the needle is rotated for 20^o, and at step 15, the needle is rotated for another 200^o. Fig. 7 shows the bevel-tip flexible needle insertion in the 3D soft tissue.

VI. Conclusions and Future Work

In this paper, we presented a framework to model and simulate flexible needle insertion through soft tissue in a different way from the classic FEM-based approaches. Both the tissue and needle are modeled using two set of nodes, which are no longer constrained by mesh as in FEM-based approaches. All nodes are connected by influence domains of their local neighbors using a moving least square approximation. During the insertion, new nodes will be added into

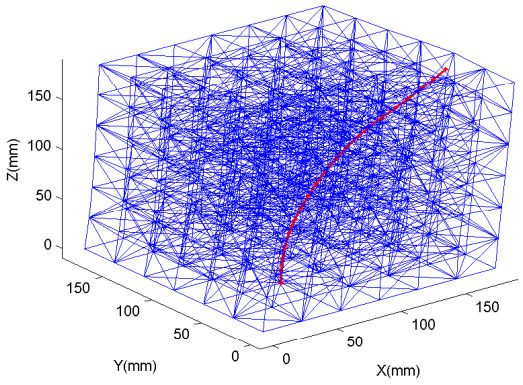

(a) step 20

Fig. 7. Flexible needle insertion in 3D soft tissue.

the tissue by exactly following the needle's kinematics or dynamics. Interactions between the needle and tissue can be calculated and simulated through their influence domains. Different from FEM-based approaches which require mesh modification or local remeshing to approximate the needle's trajectory, the meshfree approach allows higher numerical accuracy of the simulation [26]. Therefore, this framework has high potential to be combined with motion planning approaches that requires exact agent dynamics and environment information, such as Probabilistic Roadmap (PRM) or the Rapidly-exploring Random Trees (RRT), to plan accurate insertion of the flexible needle in soft tissue in future works.

In this paper, we only considered elastic soft tissues that are isotropic, and linear. However, once realistic material properties can be obtained through experiments in future work, they can be applied straightforwardly to this meshfree approach. We will also consider soft tissues with complicated geometry and develop adaptive node distribution to better represent regional properties. Based on this framework, we will also pursue motion planning for flexible needle insertion in both 2D and 3D environments.

REFERENCES

[1] V. Duindam, R. Alterovitz, S. Sastry, and K. Goldberg, "Screw-based motion planning for bevel-tip flexible needles in 3d environments with obstacles," in *Proceedings of IEEE International Conference on Robotics and Automation*, 2008, pp. 2483–2488.

[2] J. Xu, V. Duindam, R. Alterovitz, and K. Goldberg, "Motion planning for steerable needles in 3d environments with obstacles using rapidly-exploring random trees and backchaining," in *Proceedings of IEEE International Conference on Automation Science and Engineering*, 2008.

[3] ——, "Planning "fireworks" paths for medical steerable needle insertion to reduce trauma on patients," *Proceedings of IEEE/RSJ International Conference on Intelligent Robots and Systems*, 2009.

[4] S. Rodriguez, J. Lien, and N. Amato, "Planning motion in completely deformable environments," *Proceedings of IEEE International Conference on Robotics and Automation*, 2006.

[5] K. J. Bathe, *Finite Element Procedures*. Prentice Hall, 1996.

[6] T. Belytschko, Y. Krongauz, D. Organ, M. Fleming, and P. Krysl, "Meshless methods: an overview and recent developments," *Computer Methods in Applied Mechanics and Engineering*, vol. 139, no. 1-4, pp. 3–47, 1996.

[7] R. J. Webster III, J. S. Kim, N. J. Cowan, G. S. Chirikjian, and A. M. Okamura, "Nonholonomic modeling of needle steering," *International Journal of Robotics Research*, vol. 5/6, pp. 509–525, 2006.

[8] R. J. Webster III, J. Memisevic, and A. M. Okamura, "Design consideration for robotic needle steering," in *Proceedings of IEEE International Conference on Robotics and Automation*, 2005.

[9] R. Alterovitz, A. Lim, K. Goldberg, G. S. Chirikjian, and A. M. Okamura, "Steering flexible needles under markov motion uncertainty," in *Proceedings of IEEE/RSJ International Conference on Intelligent Robots and Systems*, 2005, pp. 120–125.

[10] R. Alterovitz, M. Branicky, and K. Goldberg, "Constant-curvature motion planning under uncertainty with applications in image-guided medical needle steering," in *Proceedings of workshop on the Algorithmic Foundations of Robotics*, 2006.

[11] R. Alterovitz, T. Siméon, and K. Goldberg, "The Stochastic Motion Roadmap: A sampling framework for planning with Markov motion uncertainty," in *Robotics: Science and Systems*, 2007.

[12] V. Kallen and N. J. Cowan, "Image-guided control of flexible beveltip needles," in *Proceedings of IEEE International Conference on Robotics and Automation*, 2007, pp. 3015–2020.

[13] W. Park, J. S. Kim, Y. Zhou, N. J. Cowan, A. M. Okamura, and G. S. Chirikjian, "Diffusion-based motion planning for a nonholonomic flexible needle model," in *Proceedings of IEEE International Conference on Robotics and Automation*, 2005, pp. 4611–4616.

[14] V. Duindam, J. Xu, R. Alterovitz, K. Goldberg, and S. Sastry, "3d motion planning algorithms for steerable needles using inverse kinematics," in *Proceedings of International Workshop on Algorithmic Foundations of Robotics*, 2008.

[15] S. DiMaio and S. Salcudean, "Needle insertion modeling and simulation," *IEEE Transactions on Robotics and Automation*, no. 5, pp. 864–875, 2003.

[16] D. Magee and D. Kessel, "A computer based simulator for ultrasound guided needle insertion," in *IEE International Conference on Visual Information Engineering*, 2005, pp. 301–308.

[17] S. Jiang, N. Hata, and R. Kikinis, "Needle insertion simulation for image-guided brachytherapy of prostate cance," in *The 2nd International Conference on Bioinformatics and Biomedical Engineering*, 2008.

[18] H. Nienhuys and A. V. der Stappen, "Interactive needle insertions in 3d nonlinear material," Institute of Information and Computing Sciences, Utrecht University, Tech. Rep., 2003.

[19] A. Wittek, T. Dutta-roy, Z. Taylor, A. Horton, T. Washio, K. Chinzei, and K. Miller, "Subject-specific non-linear biomechanical model of needle insertion into brain," *Computer Methods in Biomechanics and Biomedical Engineering*, vol. 11, no. 2, pp. 135–146, 2008.

[20] R. Alterovitz, J. Pouliot, R. Taschereau, I.-C. Hsu, and K. Goldberg, "Needle insertion and radioactive seed implantation in human tissues: Simulation and sensitivity analysis," in *Proceedings of IEEE International Conference on Robotics and Automation*, 2003.

[21] R. Alterovitz, K. Goldberg, J. Pouliot, and I.-C. Hsu, "Sensorless motion planning for medical needle insertion in deformable tissues," *IEEE Trans. Information Technology in Biomedicine*, vol. 13, no. 2, pp. 217–225, 2009.

[22] N. Chentanez, R. Alterovitz, D. Ritchie, L. Cho, K. K. Hauser, K. Goldberg, J. R. Shewchuk, and J. F. O'Brien, "Interactive simulation of surgical needle insertion and steering," in *Proceedings of ACM SIGGRAPH 2009*, Aug. 2009.

[23] B. Dunkin, G. Adrales, K. Apelgren, and J. Mellinger, "Surgical simulation: A current review," *Surgical Endoscopy*, vol. 21, no. 3, pp. 357–366, 2007.

[24] R. Murray, Z. Li, and S. Sastry, *A Mathematical Introduction to Robotic Manipulation*. CRC Press, 1994.

[25] C. Simone and A. M. Okamura, "Modeling of needle insertion forces for robot-assisted percutaneous therapy," in *IEEE International Conference on Robotics & Automation*, 2002, pp. 2085–2091.

[26] K. C. L. Wong, L. Wang, H. Zhang, H. Liu, and P. Shi, "Meshfree implementation of individualized active cardiac dynamics," *Computerized Medical Imaging and Graphics*, p. http://dx.doi.org/10.1016/j.compmedimag.2009.05.002, In press.